Science Advances

AAAS

advances.sciencemag.org/cgi/content/full/2/1/e1501054/DC1

Supplementary Materials for

Two-photon quantum walk in a multimode fiber

Hugo Defienne, Marco Barbieri, Ian A. Walmsley, Brian J. Smith, Sylvain Gigan

Published 29 January 2016, *Sci. Adv.* **2**, e1501054 (2016)
DOI: 10.1126/sciadv.1501054

The PDF file includes:

1. Experimental details

Characterisation of the maximum indistinguishability of the photon pairs

A 10 mm long periodically-poled potassium titanyl phosphate (PPKTP) crystal pumped with a 25 mW continuous-wave laser diode at 405 nm central wavelength produces pairs of frequency-degenerate photons by a type-II SPDC process. Both photons are filtered using narrowband filters centred at 810nm (FWHM = 1 nm), yielding a coincidence rate of up to 6×10^4 counts/s. The maximum indistinguishability of the pair is measured by performing a Hong-Ou-Mandel experiment (*36*). The experimental setup is represented on Fig.S1a. The coincidence curve obtained by scanning the path length difference of the two photons is shown on Fig.S1b. We measure a visibility of 86%.

Temporal dispersion in the multi-mode fibre

When polychromatic light propagates in an optical waveguide spectral dispersion influences the temporal evolution and has three primary origins: chromatic dispersion, group velocity dispersion and modal dispersion. Working with a multimode fibre (MMF), modal dispersion is the main contributing source of dispersion (*43*). It describes the phenomenon in which the different modes supported in a MMF experience different delays along the propagation because of the different paths that they follow. This type of dispersion leads to the broadening of the initial temporal profile of the input light. While we do not control the temporal degree of freedom in this experiment (*40, 41*), characteristics of the MMF have been chosen to have negligible spectral dispersion considering the 1 nm bandwidth of the photons.

In our experiment, we used a graded-index MMF with a core diameter of 50 μm and a total length of 11 cm. The fiber dispersion can be characterized using the setup in Fig.S2a. The photon-pair source is replaced by a superluminescent diode (SLED) filtered using the same 1 nm bandpass filter. Part of the light entering the MMF after refection on SLM H creates an output speckle (Speckle A) that can interfere with the speckle created by the part of the light reflected by SLM V (Speckle B). Interference appears only if the path length difference δ between the two parts is close to $\delta = 0$. By choosing an output position (speckle grain) where both speckles have the same intensity, interference fringes recorded on Fig.S2b using the 11 cm long MMF shows a contrast value close to unity, indicating that the fiber dispersion is then negligible. As a comparative example, dispersion is clearly visible on Fig.S2c showing an interference pattern recorded using the 1 m long graded index MMF with a core diameter of 62.5 μm and a 3 nm bandpass filter. This pattern has a contrast value of 65%, far from unity, corresponding to significant temporal distortion.

Transverse optical modes supported by the multimode fiber

In our experiment, we use a 11-cm long graded index multimode fibre (MMF) with core diameter d = 50 μm, an index profile parameter of g = 2 (corresponding to a parabolic index profile) and a numerical aperture of $NA_0 = 0.2$. The number of optical modes supported by a graded index MMF at $\lambda = 810$ nm can be evaluated as (*1*)

$$N_f \approx \frac{g}{2(g+1)}\left(\frac{\pi\, NA_0}{\lambda}\right)^2 \qquad (1)$$

which returns a value of $N_f \approx 380$ modes.

2. Controlling the two-photon field using the two-photon transmission matrix

Control of photon-pairs propagation

The transmission matrix (TM) of the MMF is measured using a classical light source, a superluminescent diode (SLED) filtered with the same band-pass filter as that used with the photon pair source (810 ± 1 nm). Scanning input field distributions with SLM H and SLM V permits measurement of the TM relative to both input polarization modes (*37*). The output fields are measured with a holographic method using a unique reference field. The transmission matrix T of an optical system is the M × N matrix that connects N modes of an input field to M modes of an output field. Here, T has been determined using an input field decomposed into N = 370 input modes, corresponding to N_H = 180 modes controlled by SLM H and N_V = 190 modes controlled by SLM V. At the end of the process, T is projected onto the SLM pixel basis using a change of basis multiplication.

Propagation of n indistinguishable photons through a complex multimode system can be described using the n-photon transmission matrix denoted $T^{(n)}$. This matrix transforms any n-photon input state to its corresponding n-photon output state. Propagation of a two-photon state in a MMF, characterized by a N-input × M-output transmission matrix T, can then be described using the two-photon transmission matrix $T^{(2)}$. A matrix coefficient $\Gamma_{i_1,i_2}^{j_1,j_2}$ of $T^{(2)}$ connects a two-photon input state $|1_{i_1} \dots 1_{i_2}\rangle$, containing one photon in mode i_1 and one photon in mode i_2 (with $\{i_1 \leq i_2\} \in [1, N]$), to a two-photon output state $\langle 1_{j_1} \dots 1_{j_2}|$, containing one photon in mode j_1 and one photon in mode j_2 (with $\{ j_1 \leq j_2\} \in [1,M]$). This coefficient is calculated using matrix coefficients of T relative to the corresponding modes. The analytic expression relating the two-photon transmission matrix element and the transmission matrix of the classical field is given by

$$\Gamma_{i_1,i_2}^{j_1,j_2} = \frac{t_{j_1,i_1}t_{j_2,i_2} + t_{j_1,i_2}t_{j_2,i_1}}{\sqrt{(1+\delta_{i_1,i_1})(1+\delta_{j_1,j_2})}}$$

where $t_{i,j}$ represents the ijth matrix element of T connecting input mode i to output mode j and $\delta_{i,j}$ is the Kronecker delta, which equals to 1 if $i = j$ and 0 otherwise (*44*).

As detailed in (*37*), the transpose conjugate of T can be used to control light propagating in a complex system. In this work, the same method is applied to the two-photon transmission matrix $T^{(2)}$ to maximize coincidences between two arbitrarily selected output states $|X\rangle$ and $|Y\rangle$. The targeted two-photon output state can be formally written $|\psi_{\text{tar}}\rangle = a_X^\dagger a_Y^\dagger |0\rangle$. The corresponding input state $|\psi_{\text{foc}}\rangle$ is determined using T_2^+:

$$|\psi_{\text{foc}}\rangle = T_2^+ |\psi_{\text{tar}}\rangle = \sum_{\{i_1,i_2\}\in[1,N]} \left(\Gamma_{i_1,i_2}^{X,Y}\right)^* |1_{i_1} \dots 1_{i_2}\rangle$$

Therefore, $|\psi_{\text{foc}}\rangle$ represents the two-photon input state that needs to be prepared at the input to observe $|\psi_{\text{tar}}\rangle$ at the output. Due to experimental constraints, the system realized does not permit perfect shaping of the two-photon input state. As described in Fig.1, two independent parts of a phase only spatial light modulator (SLM H and SLM V) are used to shape the input field. This specific experimental configuration presents three limitations:

- Each photon of the pair has access only to a limited number of input states. SLM V shapes one photon over a set of vertical polarization modes of the MMF and SLM H over a set horizontal polarization modes. Because one part of the SLM cannot distribute the photon over the modes accessible to the other, we have to distinguish two distinct sets of input states denoted Ω_H and Ω_V discriminating states controlled by SLM H and SLM V ($\dim(\Omega_H) = N_H$ and $\dim(\Omega_V) = N_V$).

- The complete two-photon input state has a factorized form. Because each photon is shaped independently by two distinct parts of the SLM, the resulting two-photon field is a product of fields associated with each photon.
- Phase-only SLMs can only control phase of the shaped field and not its amplitude. When the input state is expressed in the SLM pixel basis – one input mode corresponds to one SLM pixel - the SLM acts only on the phase component of each mode.

Taking into account these experimental limitations, the most general input state that can be generated is written as

$$|\psi_{\text{slm}}\rangle = \frac{1}{\sqrt{N_H\, N_V}}\left(\sum_{i_1\in\Omega_H} e^{i\,\phi_{i_1}}\, a_{i_1}^{\dagger}\right)\left(\sum_{i_2\in\Omega_V} e^{i\,\phi_{i_2}}\, a_{i_2}^{\dagger}\right)|\emptyset\rangle$$

where ϕ_i represent a phase parameter associated with input mode i. Note that this expression of the input state is written in the SLM pixels basis where an input mode i represents a pixel – or a macropixel- of the SLM. Because of the strong mode coupling in the MMF, these limitations do not affect the random characteristic of the quantum walk, each photon being equally spread out over all the output modes.
In our study, we isolated two possible input states that approach as best as possible the ideal state $|\psi_{\text{foc}}\rangle$ that allows optimizing coincidences between output states $|X_2\rangle$ and $|Y_3\rangle$. These two input states denoted $|\psi_1\rangle$ and $|\psi_2\rangle$ correspond to the two experimental configurations represented in Fig.3. They take the analytical forms

$$|\psi_1\rangle = \frac{1}{\sqrt{N_H\, N_V}}\left(\sum_{i_1\in\Omega_H} \arg(t^{*}_{X_2,i_1})\, a_{i_1}^{\dagger}\right)\left(\sum_{i_2\in\Omega_V} \arg(t^{*}_{Y_3,i_2})\, a_{i_2}^{\dagger}\right)|\emptyset\rangle$$

$$|\psi_2\rangle = \frac{1}{\sqrt{N_H\, N_V}}\left(\sum_{i_1\in\Omega_H} \arg(t^{*}_{X_2,i_1} + t^{*}_{Y_3,i_1})\, a_{i_1}^{\dagger}\right)\left(\sum_{i_2\in\Omega_V} \arg(t^{*}_{X_2,i_2} + t^{*}_{Y_3,i_2})\, a_{i_2}^{\dagger}\right)|\emptyset\rangle$$

The overlap values between $|\psi_{\text{foc}}\rangle$ and $|\psi_1\rangle$ or $|\psi_2\rangle$ are $|\langle\psi_{\text{foc}}|\psi_1\rangle|^2 \approx 16\%$ and $|\langle\psi_{\text{foc}}|\psi_2\rangle|^2 \approx 13\%$. These overlaps quantify the impact of the experimental constraints on the efficiency of the focusing process.

Deterministic control of quantum interference
The experiment that allows controlling quantum interference in the MMF described on Fig.4 is realized using a generalised form of $|\psi_2\rangle$ introducing the set of angles $\{\phi_H, \phi_V\}$. This state takes the form

$$|\psi_2\rangle_{\phi_H,\phi_V} = \frac{1}{\sqrt{N_H\, N_V}}\left(\sum_{i_1\in\Omega_H} \arg(t^{*}_{X_2,i_1} e^{i\,\phi_H} + t^{*}_{Y_3,i_1})\, a_{i_1}^{\dagger}\right)\left(\sum_{i_2\in\Omega_V} \arg(t^{*}_{X_2,i_2} e^{i\,\phi_V} + t^{*}_{Y_3,i_2})\, a_{i_2}^{\dagger}\right)|\emptyset\rangle$$

The non-classical contrast is defined as $C = (R_{\delta=0} - R_{\delta=0.4mm})/R_{\delta=0.4mm}$, where $R_{\delta=0}$ ($R_{\delta=0.4mm}$) is the two-photon coincidence rate at zero (0.4 mm) path length difference between input photons.

Contrast values in output state $\hat{a}^{+}_{|X_2\rangle}\hat{a}^{+}_{|Y_3\rangle}|0\rangle$ are measured in Fig.4a for 64 different relative phase settings (φ_H , φ_V).

Experimental values of Fig4.a fit with a confidence of 95% to a theoretical model of the form $A\cos(\phi_H - \phi_V + B)$ with parameters A = 0.71 and B = −0.4rad. A represents the maximum contrast accessible by the photon pairs propagating in the MMF (close to the ideal value of 86% measured with the HOM experiment) and B the relative phase offset made during the matrix measurement process.

3. Validation of the experimental data

Measurements realized in our study require long acquisition time and therefore long-term stability of the system. Due to temperature fluctuations and mechanical vibrations, conformation of the MMF evolves with time and the speckle pattern changes. Stability of the MMF is monitored during the measurement process by correlating the output speckle pattern at regular time intervals. In all results presented here, a lower limit for the correlation of 85% has been observed.

We conduct a statistical analysis of our data to assess the error on the measured contrast. Poisson statistics (mean value and standard deviation denoted respectively μ and σ) is an appropriate model for our counting experiment. Considering the number of measurements N_{meas} = 90 > 30, this distribution can be approximated by a Gaussian. The estimators associated with μ and σ are respectively denoted $\overline{\mu}$ and $\overline{\sigma}$. Experimental values divided by the number of measurements N_{meas} represent a direct estimation of μ. The standard deviation of this estimator, which corresponds to its 65% confidence interval, is given by

$$\sigma_{\overline{\mu}} \approx \frac{\overline{\sigma}}{\sqrt{N_{\text{meas}}}}$$

$\overline{\sigma}$ is calculated from experimental data as $\overline{\sigma}^2 = 1/N_{\text{meas}} \sum_{i=1}^{N_{\text{meas}}} (X_i - \overline{\mu})$ where X_i is the number of coincidences measured during the *i*-th measurement. Data presented in the manuscript have been analyzed with this statistical tool. Fig.S3 represents the relative standard deviations associated with measurements of Fig.2.

While a limited number of coincidence measurements present a high uncertainty value, due to their low intensity, the average error values for matrices measured with distinguishable and indistinguishable photons are below 10%. Average standard deviation on the non-classical contrast matrix is about ±0.22. Data acquired are then sufficiently relevant to conclude that non-classical interference occurs in the MMF during photon propagation.

Table S1 represents data analysis of the experimental values relative to the targeted focusing state represented in Fig.3. In particular, non-classical contrast associated with each focusing configuration (respectively 0.017 and 0.72) show small errors (respectively ±0.035 and ±0.07). The role played by non-classical interference in the focusing process is clear.

Statistical data analysis of Fig.4 is represented in Fig.S4. The average error on the contrast matrix reconstructed with 8 × 8 different phase settings (Fig.4.a) is around ±0.11. Error values registered on the scans realized with three different phase settings (Fig.4.b) are below 5%.

Focussing configuration	Data Type	Measured value	Standard deviation
First focussing configuration (Fig.3a1)	Coincidences with distinguishable photons in 900s (Fig.3a2)	7949	2.1%
	Coincidences with distinguishable photons in 900s (Fig.3a3)	8088	1.3%
	Contrast	0.017	0.035
Second focussing configuration (Fig.3b1)	Coincidences with distinguishable photons in 900s (Fig.3a2)	3491	2.3%
	Coincidences with distinguishable photons in 900s (Fig.3a3)	6038	1.8%
	Contrast	0.72	0.07

Table S1: Statistical analysis of experimental data presented in Fig. 3. Coincidences and non-classical contrast relative to the targeted output focusing state show a very good confidence in the results. In particular, non-classical contrasts associated to each focusing configuration (respectively 0.017 and 0.72) present very small relative errors (respectively ±0.035 and ±0.07).

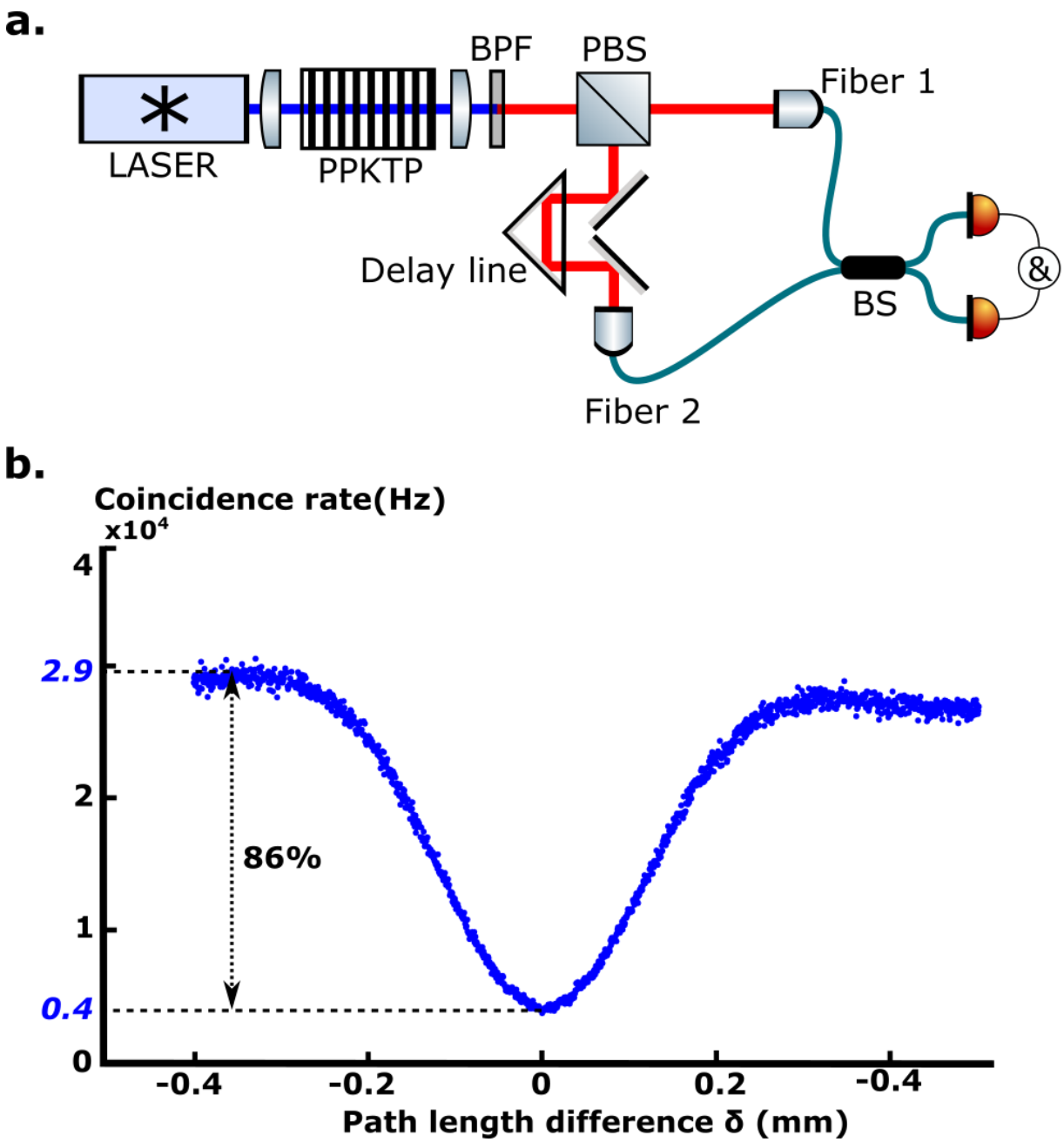

Figure S1: Characterisation of the photon-pair indistinguishability by the Hong-Ou-Mandel experiment. (a.) represents the apparatus designed to generate photon pairs and measure their visibility. A 10 mm PPKTP crystal pumped with a 25 mW continuous-wave laser diode at 405 nm produces pairs of photons by a type-II Spontaneous Parametric Down Conversion (SPDC) process. Both photons are filtered using a 1nm bandpass filter centered at 810 nm (BPF) yielding a coincidence rate up to 6×10^4 1/s and a coupling ratio around 9%. After separating them using a polarizing beam splitter (PBS), they are injected in a balanced beam splitter (BS). **(b.)** We observe a dip in the coincidences curve recorded by monitoring the path length difference δ between the photons. The visibility measured is about 86%.

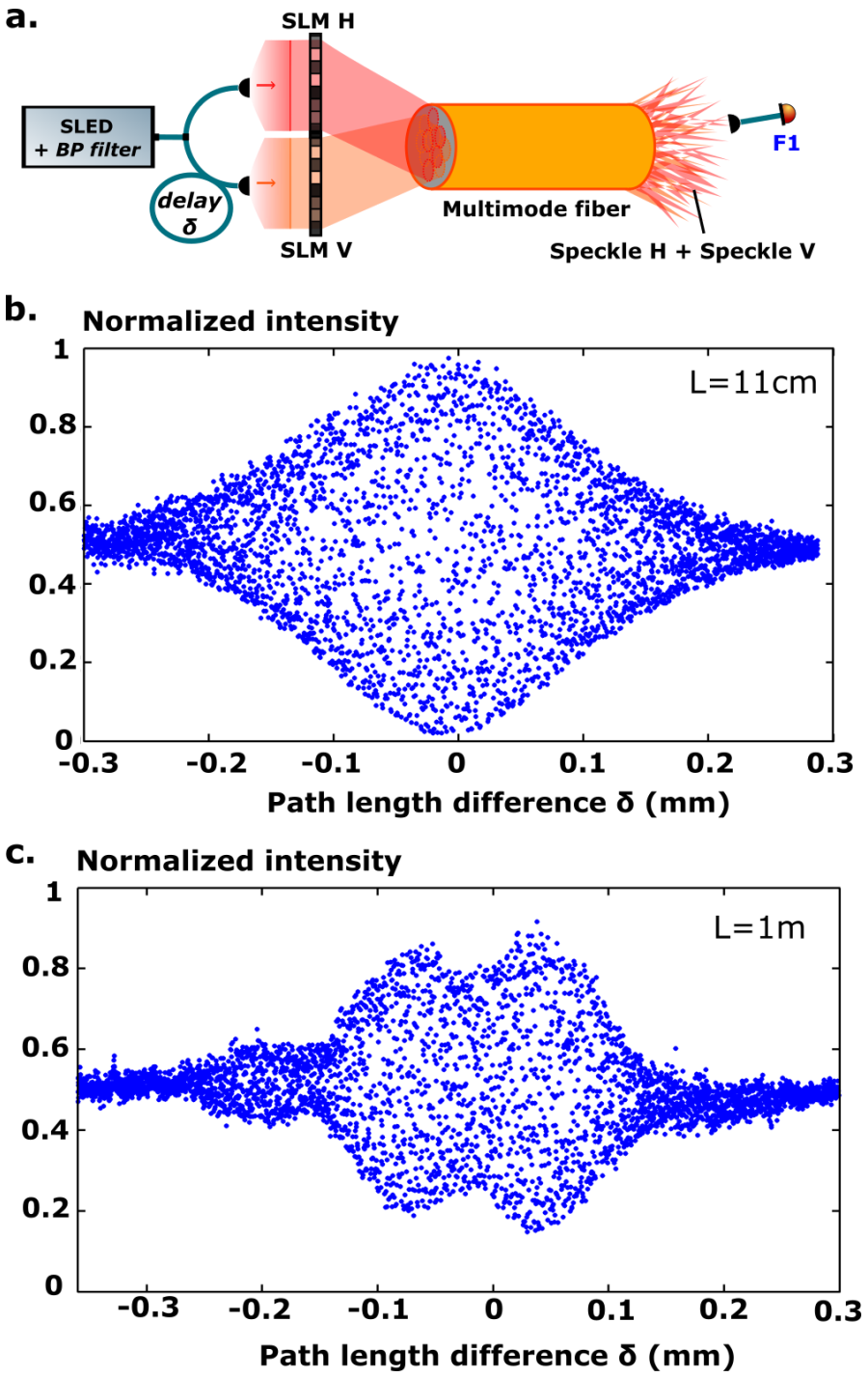

Figure S2: Dispersion characterization through the MMF. (a.) represents the experimental configuration used to characterize the dispersion in the MMF. Light coming from the SLED is filtered out and split in two parts. Each part is injected into the MMF using SLM H or SLM V. Combination of the two corresponding speckles created after propagation in the MMF are measured at a specific output position using fiber F1 and interference fringes are recorded by monitoring the path length difference δ. Interferences pattern measured with a 11 cm long graded-index MMF with a core diameter of 50 μm **(b.)** and a SLED filtered with a 1nm bandpass filter permits to extract a contrast value about 95%. Temporal dispersion is then negligible. As a comparative example,

interferences fringes recorded using a 1m long graded-index MMF with a core diameter of 62.5 µm **(c.)** and a SLED filtered with a 3 nm bandpass presents a strong temporal distortion and a contrast reduced to 65%.

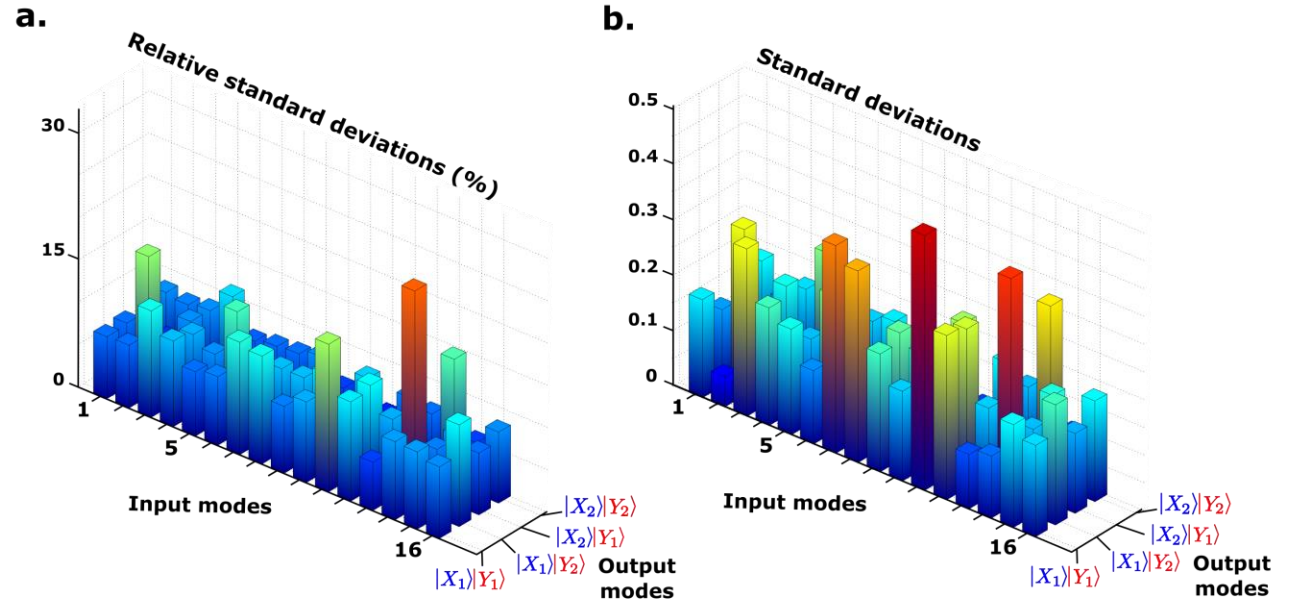

Figure S3: Statistical analysis of experimental data represented on Fig. 2. (a.) Relative standard deviation associated to the matrix values measured with indistinguishable photons. The average error value over the matrix is equal to 8.9%. **(c.)** Standard deviation associated to the non- classical contrast matrix. The average error value over the matrix is equal to 0.22.

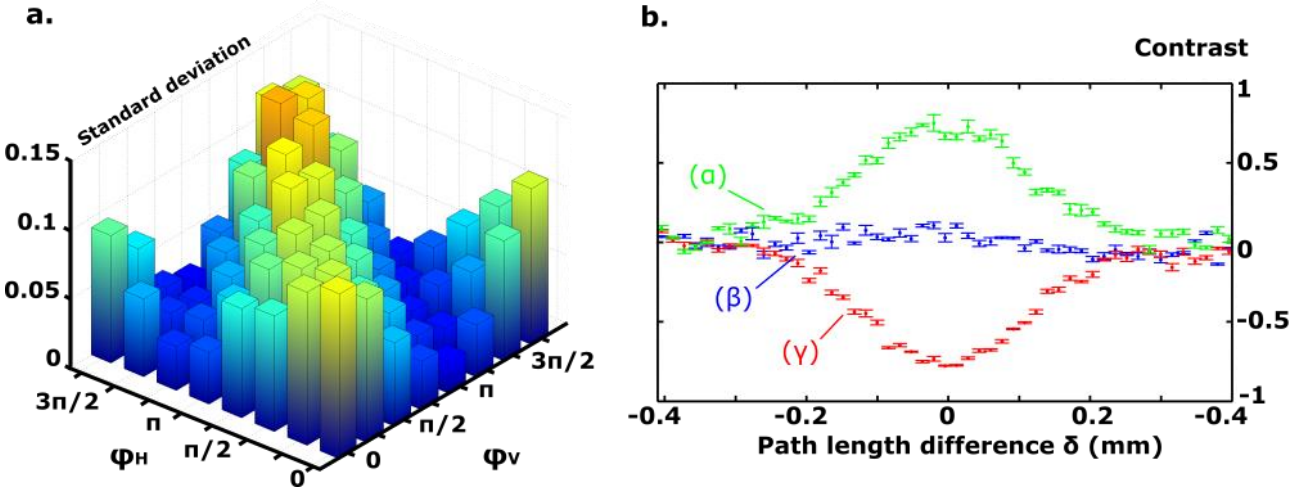

Figure S4: Statistical analysis of experimental data presented on Fig. 4. **(a)** Standard deviation of contrast matrix measured with 8 × 8 = 64 phase settings (Fig.4.a). **(b)** Contrast values and corresponding error bars for three phase settings as a function of the path length difference between input photons δ (Fig.4.b).